arXiv:1702.06708v1 [cond-mat.mes-hall] 22 Feb 2017

# Layer-Pressure Topological Phase Diagram of Few-Layer Phosphorene

Peng-Lai Gong,[1,2] Bei Deng,[1] Liang Hu,[1] Wei-Chao Wang,[2] Da-Yong Liu,[3,*] Xing-Qiang Shi,[1,†] Zhi Zeng,[3,4] and Liang-Jian Zou[3,4,‡]

[1] *Department of Physics, Southern University of Science and Technology, Shenzhen 518055, China*
[2] *Department of Electronics and Tianjin Key Laboratory of Photo-Electronic Thin Film Device and Technology, Nankai University, Tianjin 300071, China*
[3] *Key Laboratory of Materials Physics, Institute of Solid State Physics, Chinese Academy of Sciences, P. O. Box 1129, Hefei 230031, China*
[4] *University of Science and Technology of China, Hefei 230026, China*

A layer-pressure topological phase diagram is obtained for few-layer phosphorene under increasing hydrostatic pressures by first-principles electronic structure calculations. We show that pressure can *effectively* manipulates the band structures of few-layer phosphorene — a pressure of less than 4.2 GPa can drive the quasi-two-dimensional (2D) phosphorene (of 4 layers or thicker) from normal insulators to nontrivial topological Dirac semimetals (TDSMs). Such 2D TDSMs phase possesses a single pair of Dirac cones *exactly* at the Fermi level, in startling contrast to the pressured *bulk* black phosphorous (BP) which has hole- and electron-types Dirac cones mixed with normal fermions. The band gap $E_g$ and its change rate with pressure $dE_g/dP$ show a clear size-dependence on the thickness along the interlayer vertical direction, which are related to the quantum confinement effect (QCE). Although the QCE in 2D phosphorene makes the band inversion occur at a higher pressure with respect to the bulk, it becomes less important in thicker layers. Our results show that pressured few-layer phospherene is more suitable for electronic applications than *bulk* BP.

Topological insulators (TIs) and semimetals (TSMs) are new states of quantum matters. TI is different from normal insulator (NI) in a sense that it is insulating in the bulk, while the surface of 3-dimensional (3D) TI or the edge of 2-dimensional (2D) TI supports metallic or conducting electronic states [1–5]. TSMs, including topological Dirac semimetals (TDSMs) [6, 7], Weyl semimetals [8–11] and node-line semimetals [12], possess zero or low density of states near the Fermi level ($E_F$). TDSMs can transform into Weyl semimetals when the time-reversal symmetry or inversion symmetry is broken. Also, 3D TDSMs, consider for example, $Na_3Bi$ [6], $Cr_3As_2$ [13] and CaTe [14], can be converted into various topological phases by explicit breaking of symmetries. Thus, TDSMs can be regarded as a bridge to other topological or nontrival phases. Recently, Cava *et al.* have claimed that a crystal with glide planes and/or screw axes might form a 3D Dirac semimetal if this crystal possesses a twofold-degenerate energy band, since the nonsymmorphic symmetry in the lattice could lead to the band crossing in the Brillouin zone [15]. In recent years, black phosphorus (BP) have received considerable interest due to its exotic properties [16–19]. *Bulk* BP, with a direct band gap of ∼0.3 eV [20], has glide planes and screw axes. Thus it is a candidate of a 3D Dirac semimetal under some external controls.

Multilayer BP can transform from normal semiconducting phase to nontrival topological phases via an external electric field [21, 22] or carrier doping [23]. Zunger *et al.* have pointed out that few-layer phosphorene can experience a topological phase transition (TPT) from normal insulators to nontrivial topological materials (including TIs and topological metals) via an external electric field (of $> 0.7$ V/Å) in a 4-layer phosphorene [21]. Unfortunately, such large external electric field is very difficult to realize in real applications. Also, Kim *et al.* have observed the Dirac semimetal state by depositing K ions on the surface of few-layer phosphorene, but the observed topological Dirac points (with a tiny gap of ∼10 meV along the armchair direction) actually locate at ∼0.5 eV below $E_F$, due to the electron-doping of potassium ions to the host material [23]. The heavy electron-doping in the Dirac semimetal cannot take full advantage of massless Dirac fermions in transport or optical devices. In addition, a pure TDSMs phase cannot be realized by the above mentioned methods, probably due to the symmetry broken by the electric field or dopants. In the current work, we show that hydrostatic pressure is a more efficient (a moderate pressure of $P$<4.2 GPa) and better (Dirac points just at $E_F$) way to activate the topological phase transitions in few-layer phosphorene. Very recently, we have reported that *bulk* BP can convert from a NI into a 3D Dirac semimetal under a hydrostatic pressure of ∼1.20 GPa [18, 19], which makes *bulk* BP serve as a new building block for the study of TPTs. In the 2D cases, due to the reduced dimension, extra novel phenomena would take place [24, 25]. However, for 2D phosphorene, there remains a lack of study regarding their topological properties and topological phase diagram as a function of pressure and number of layers.

In this Letter, the layer-pressure topological phase diagram of few-layer phosphorene is obtained [with spin-orbital coupling (SOC) effect] (Fig. 2). We discovered that pressures can drive the 2D phosphorene from NIs to pure TDSMs (namely, with only Dirac fermions at $E_F$ [Fig. 3(c)]), with the TPTs strongly depending on the

number of layers and pressures. Below the critical pressure, the 2D phosphorene remains NIs for $n$ = 2 and 3 layers. For $n$ = 4-6 layers, they undergo TPTs from NIs to TDSMs when the pressure exceeding $P_C$ ($P_C$ is the critical pressure of electronic phase transitions from NI to TDSM). Such a 2D pure TDSM phase is found to possess a single pair of Dirac points, which are protected by the nonsymmorphic space symmetry (glide plane) in few-layer phosphorene and thus can not be opened up by SOC. The underlying mechanism for the band-gap reducing, closing and band inversion under pressure is attributed to the increasing of interlayer coupling induced by pressures. The band gap $E_g$ and its change rate $dE_g/dP$ show a clear size-dependence on the thickness along the interlayer vertical direction, owing to the quantum confinement effect [26]. The critical pressure for the band inversion is increased by about 50% due to the quantum confinement effect in 4-layer phosphorene, but this effect will be significantly reduced to 33% in 6-layer phosphorene (see Fig. S2 (c) in the Supplemental Material [27].

Few-layer BP is a layered material, in which each layers stackes together by van der Waals (vdW) interactions. Each layer consists of two sublayers and in turn forms a bulking honeycomb structure. The structural model of 2-layer phosphorene, as a representative for a finite $n$-layer phosphorene ($n$ denotes the number of layers), is shown in Figs. 1(a) and 1(b), where the directions of lattice vectors $a$ and $b$ are along the zigzag (the $y$ axis) and the armchair (the $x$ axis) directions, respectively. The 2D rectangular Brillouin zone of $n$-layer phosphorene is shown in Fig. 1(c).

In order to explore the evolutions of electronic structures of few-layer phosphorene under increasing hydrostatic pressures, we first determine their crystal structures (under each pressure) by density functional theory (DFT) calculations. We employed the Vienna Ab initio Simulation Package (VASP) [28] with the projector augmented wave (PAW) method [28, 29]. The interlayer vdW interaction is described by the optB88-vdW functional [30]. A previous study about few-layer $MoS_2$ has proposed an extraction method to obtain the 2D structures under pressure[31]. In our study we adopt the extraction method, namely the structure of *bulk* BP was firstly optimized under a specified hydrostatic pressure, and then these structural parameters were used to construct the $n-$layer phosphorene, with a vacuum space of 20 Å along the z direction. Based on the constructed 2D structures, the electronic properties is calculated by the hybrid functional of Heyd, Scuseria, and Ernzerhof (HSE06) [32]. More calculation details can be found in the Supplemental Material [27]).

With increasing pressure, as shown in Fig. 1(d), the lattice constant $b$ (armchair direction) and the interlayer spacing between two adjacent phosphorene layers ($d_{int}$) are significantly shortened (by 5.6% and 8.8% for $b$ and $d_{int}$ at 4.0 GPa), while $a$ (zigzag direction) and the sublayer distance within one single layer ($h$) remain almost unchanged.

The thermodynamic and kinetic stabilities of few-layer phosphorene depend on their atomic and electronic properties, as well as the environment, such as pressure and temperature, etc. In the current work, the stabilities of few-layer phosphorene are similar to that of *bulk* BP. The thermodynamic stability of BP is considered through the enthalpy-pressure relationship. We find that the critical pressure of thermodynamic stability $P_T$ is 4.5 GPa (see Fig. S1 in the Supplemental Material [27]), very close to the experimental result (4.7 GPa) [33], which indicates a structural phase transition from a A17 (orthorhombic) phase to a A7 (rhombohedral) phase for *bulk* BP when $P>P_T$ [34]. For 2D phosphorene, a similar structural phase transition is found in our calculations. Phonon spectra are then calculated to judge whether or not the thermodynamically stabled structures (with $P \leq P_T$) are kinetically stable [19]. Our results show that all the pressured structures have no imaginary frequencies below $P_T$. The above results ensure that the pressured structures below 4.5 GPa are both kinetically and thermodynamically stable.

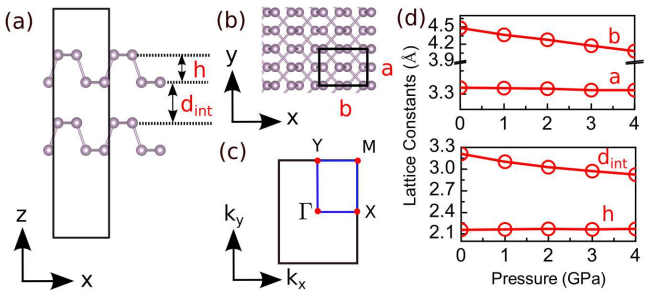


FIG. 1. (Color Online) (a) Side- and (b) top-views of the crystal structure of a 2-layer phosphorene; (c) 2D first Brillouin zone; (d) anisotropic reduction of structural parameters of few-layer phosphorene under pressure.

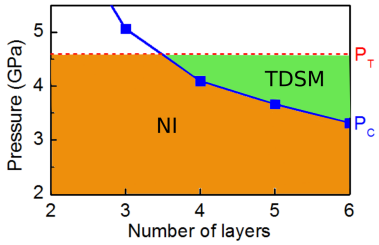


FIG. 2. (Color Online) Layer-pressure topological phase diagram of $n$-layer phosphorene. $P_C$ and $P_T$ are the critical pressures for electronic phase transition and thermodynamic stability, respectively (see text). NI denotes normal insulator [Fig. 3(a)]; and TDSM denotes a pure topological Dirac semimetal with Dirac cones just at $E_F$ [Fig. 3(c)].

*Topological phase diagram.* —The layer-pressure topological phase diagram for few-layer phosphorene (below $P_T$, with consideration of SOC) is displayed in Fig. 2, where $P_C$ and $P_T$ are the critical pressures for electronic and structural phase transitions, respectively. At $P_C$, an electronic phase transition, from NI to TDSM, takes place [Fig. 3(b)]. TDSM denotes a pure topological Dirac semimetal phase with only Dirac fermions at $E_F$ [Fig. 3(c)]. No TPTs are observed for $n = 2$ and 3 layers so they are still NIs below $P_T$ (dashed red line), this is because of their large band gaps ($\geq 0.75$ eV) under zero pressure. With increasing number of $n$, their zero-pressure band gaps gradually decrease, and a NI to TDSM transition happens to occur in the pressure range of $P_C$<$P$<$P_T$ for $n \geq 4$.

Under pressure-free conditions, 4-layer phosphorene is a semiconductor with a band gap of 0.63 eV as shown in Fig. 3(a). With increasing pressure, at $P_C = 4.1$ GPa, the valance band maximum (VBM) and conduction band minimum (CBM) touch together at Γ point of the Brillouin zone, as shown in Fig. 3(b). When $P = 4.4$ GPa, VBM and CBM with opposite parities have been inverted and a single pair of Dirac cones along Γ$Y$ (and the opposite direction of Γ$Y$) are formed [Figs. 3(c,d) and Fig. S5 in the Supplemental Material [27]], implying of a quasi-2D TDSM.

By examining the real space distribution of VBM and CBM at Γ point, we find that the two bands are really inversed when $P$>$P_C$ [Fig. 4(a)], supporting the topological phase transition. The $Z_2$ topological invariant is calculated to further check whether the band structure with band inversion is topologically nontrivial or not. The calculation is carried out following the method developed by Fu and Kane [5], based on the fact that inversion symmetry holds for all $n$-layer phosphorene studied here (see Table. S2 of the Supplemental Material [27]). The $Z_2$ topological invariant is then obtained from the parity of each pair of Kramer's degenerate occupied band at the time-reversal-invariant momenta (TRIM) points. As shown in Fig. 1(c), the BZ of $n$-layer phosphorene is a rectangle with four TRIM points: the Γ point, the X point, the M point and the Y point. The $Z_2$ topological invariant is thus expressed by,

$$\delta(\mathrm{K}_i) = \prod_{m=1}^{N} \xi_{2m}^{i}$$
$$(-1)^{\nu} = \prod_{i=1}^{4} \delta(\mathrm{K}_i) = \delta(\Gamma)\delta(\mathrm{X})\delta(\mathrm{M})\delta(\mathrm{Y}).$$

where $\delta(\mathrm{K}_i)$ stands for the product of parity eigenvalues at the TRIM points, $\xi = \pm 1$ are the parity eigenvalues and $N$ denotes the number of the degenerated occupied bands. Our results show that the band structure with band inversion has a non-zero integer $Z_2$ topological invariant ($\nu$=1), which ensures a nontrivial topological state. For different few-layers with $n$=4-6 analogically behaviors appears, namely they possess a single pair of Dirac cones with nontrivial topological $Z_2$ character when $P_C$<$P$<$P_T$.

*Quantum confinement effect in band inversion.* —As shown in Fig. 4(b), the band gap $E_g$ decreases linearly with the increasing pressure, and eventually closes at a critical pressure $P_C$ for $n \geq 4$ cases. Moreover, $P_C$ also decreases with the increase of thickness, indicating that the TDSM phases could be more realizable in thicker layers. The slope $dE_g/dP$ is calculated to be 0.23 eV/GPa for *bulk* BP (the dashed line in Fig. 4 (b)), while it is 0.17, 0.16, and 0.15 eV/GPa for 6-, 5- and 4-layer phosphorene, respectively(the solid lines in Fig. 4 (b)). The decreased $dE_g/dP$ here leads to the band-gap closing at a slower rate in few-layer phosphorene than that in the bulk. The decreased $dE_g/dP$ is supposed to be attributed to the quantum confinement effect (QCE) [26] in few-layer phosphorene. To verify this, we then confirmed that, in a given pressure range (0-1 GPa, for instance), the band gap change rate $dE_g/dP$ shows a clear size-dependence on the thickness along the $z$ direction, showing that in addition to the QCE dependence of the band gap $E_g$ (larger $E_g$ for thinner layers), the $dE_g/dP$ is also QCE-dependent, namely, smaller $dE_g/dP$ for thinner layers (see Figs. S2 (a) and (b) in the Supplemental Material [27]). The smaller $dE_g/dP$ associated with QCE resists the band-gap reduction, which, together with the QCE-induced larger gap, gives rise to a relatively larger $P_C$ (3.0 GPa) in 6-layer than that (∼1.20 GPa) in *bulk* BP [18, 19].

It was reported that the band gap of monolayer and multilayer BP can be related to the interlayer coupling

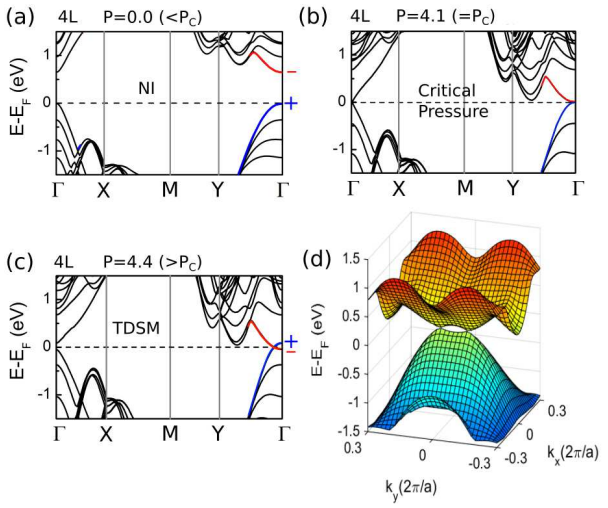


FIG. 3. (Color Online) Band structures with SOC of 4-layer phosphorene as an example at increasing pressures of (a) 0.0 GPa, (b) 4.1 GPa, and (c) 4.4 GPa; and (d) also at 4.4 GPa but the band structure is plotted in 3D for the topological Dirac semimetal (TDSM) bands around Γ point. The parity (even: +, odd: -) of VBM and CBM at Γ point is labeled in (a) and (c).

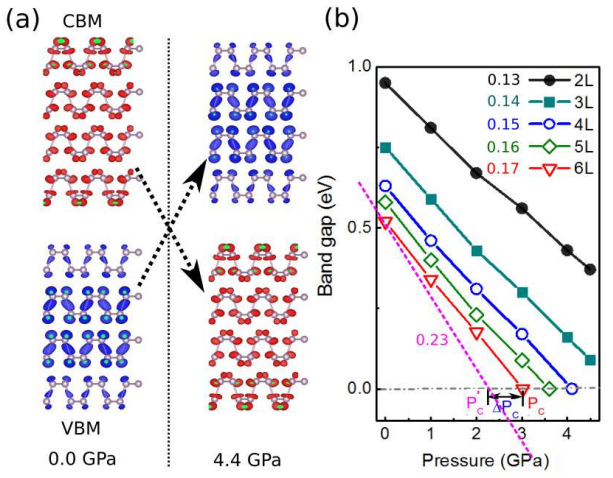


FIG. 4. (Color Online) (a) Real space distribution of VBM and CBM at Γ point under 0.0 and 4.4 GPa, respectively. (b) Band gaps of $n$-layer phosphorene as a function of pressure. The slope $dE_g/dP$ in units of eV/GPa is given near the legend; $P_C$ and $P_C'$ denotes the critical pressures with the inclusion and exclusion of QCE, and we define $\triangle P = P_C$-$P_C'$; $P_C$, $P_C'$ and $\triangle P$ as a function of the number of layers can be found in Fig. S2 (c) in the Supplemental Material [27]. The pink dashed line for *bulk* BP without QCE is also shown.

and intralayer hopping [35]. In the current work, the pressures can significantly shorten the interlayer spacing $d_{int}$, which can enhance the interlayer coupling and in turn reduce the band gap. Although the lattice constant $b$ along the intralayer armchair direction can also be shortened by pressures, the bond lengths of P-P along the same direction change slightly ($< 1\%$), so that the intralayer hopping has minor effect on the variation of band gap. Therefore, the underlying mechanism herein for the band-gap reducing, closing and band inversion is dominated by the strengthened interlayer coupling induced by pressures.

*From 3D mixed Fermions to 2D pure Dirac Fermions* —Cava *et al.* have proposed that a crystal with glide planes and/or screw axes might form a 3D Dirac semimetal. Bulk BP has glide planes and screw axes, and we have reported in an early recent work that bulk BP can convert from a NI into a 3D Dirac semimetal by a certain hydrostatic pressure (∼1.20 GPa), and such a 3D Dirac semimetal phase is protected by the nonsymmorphic space symmetry [18, 19]. In the quasi-2D cases, both odd- and even-layer phosphorene preserve glide planes and screw axes (see Table. S2 of the Supplemental Material [27]), and their space groups do not change under pressures. Thus it should be a candidate of a 2D Dirac semimetal, which is confirmed by the current work. We now discuss the evolution of Dirac cones from 3D *bulk* BP to 2D phosphorene and point out the symmetry elements that protect Dirac points. The 3D Dirac semimetal BP displays a loop (red solid circle) with continuous Dirac points around the Z point in BZ when SOC effect is not considered (see Fig. S3 (a) in the Supplemental Material [27]), which is in agreement with a previous theoretical study [36]. In fact, only two pairs of them (on the loop along $Z$-$M$ path) are exactly located at $E_F$, while others are located within ±0.15 eV around $E_F$ (see Fig. 3 (d) and Fig. 7 in Ref. [19]). With consideration of SOC, the single pair of Dirac cones along $Z$-$T$ path cannot be opened up due to the protection of group symmetry, while others on the loop are opened up with a gap (≤10 meV). In the 2D case, the single pair of Dirac cones are projected to the 2D BZ along the Γ-$Y$ path, because of the reduced dimensional effect, *i.e.*, $k_z$ coordinate disappears in the 2D BZ (see Fig. S3 (b) in the Supplemental Material [27]). For the pressured *bulk* BP ($P$>1.23 GPa), it only displays a mixture phase with the combined character of trival semimetals and topological Dirac semimetals (mTTDSM), which shows normal fermions and (hole-type and electron-type) Dirac fermions [18, 19]. The mTTDSM phase in *bulk* BP originates from the stronger anisotropic momentum and the charge compensation in $k_y$-$k_z$ plane. In contrast, the $n$-layer phosphorene is able to exhibit a pure TDSM phase with a single pairs of Dirac points exactly at $E_F$ under a certain pressure range, owing to the vanishment of anisotropic momentum $k_z$ from the reduced dimensional effect.

In order to investigate which space group symmetry elements (glide plane and/or screw axis) protect the Dirac cones in few-layer phosphorene, we calculate the band structures of few-layer phosphorene with particular deformations from the structure under 4.4 GPa. Three deformations are considered, by moving the outmost P atoms by 0.1 Å along x, y and z directions, respectively (see Fig. S4 in the Supplemental Material [27]). Our results show that translations along y and z directions cannot result in Dirac cones opening, because the YZ glide plane at the middle of the zigzag chain retains (see Table. S3 and Fig. S4 (a) in the Supplemental Material [27]). Therefore, Dirac cones are protected by the nonsymmorphic space symmetry (out-of-plane glide plane) in quasi-2D phosphorene.

In summary, we present in this work that the pure topological Dirac semimetal phase (TDSM) can be achieved in few-layer phosphorene by adopting a moderate hydrostatic pressure ($P$<4.2 GPa). The electronic band structure of TDSM shows a single pair of Dirac points exactly at the Fermi level, which are protected by the nonsymmorphic space symmetry (glide plane) and thus can not be opened up by SOC. The underlying mechanism for the band inversion under pressure is attributed to the increasing of interlayer coupling induced by pressures. On the other hand, the band gap $E_g$ and its change rate $dE_g/dP$ show a clear size-dependence on the thickness along the interlayer vertical direction, owing to the quantum confinement effect (QCE). Although the QCE in few-layer phosphorene makes the

band inversion occur at a higher pressure when referring to the bulk, this effect could be less important in thicker layers. The pressure-tunable topological properties of few-layer phosphorene may allow great flexibility in design and optimization of electronic and optoelectronic devices.

The authors are very much grateful to Dr. Xian-Long Wang, Jie Zhang and Liang-Feng Huang for many helpful discussions on the subject. This work was supported by National key research and development program (Grant No. 2016YFB0901600), the NSF of China under Grant Nos. 11474145, 11334003, 11534010, the Nanshan Key Lab on Nonvolatile Memory Grant (KC2015ZDYF0003A), and the Special Program for Applied Research on Super Computation of the NSFC-Guangdong Joint Fund (the second phase).

* dyliu@theory.issp.ac.cn
† shixq@sustc.edu.cn
‡ zou@theory.issp.ac.cn

[1] M. Z. Hasan and C. L. Kane, Rev. Mod. Phys. **82**, 3045 (2010).
[2] X.-L. Qi and S.-C. Zhang, Rev. Mod. Phys. **83**, 1057 (2011).
[3] H. Weng, X. Dai, and Z. Fang, MRS Bull. **39**, 849 (2014).
[4] H. Zhang and S.-C. Zhang, Phys. Status Solidi Rapid Res. Lett. **7**, 72 (2013).
[5] L. Fu, C. L. Kane, and E. J. Mele, Phys. Rev. Lett. **98**, 106803 (2007).
[6] Z. Wang, Y. Sun, X.-Q. Chen, C. Franchini, G. Xu, H. Weng, X. Dai, and Z. Fang, Phys. Rev. B **85**, 195320 (2012).
[7] Y. Feng, Z. Wang, C. Chen, Y. Shi, Z. Xie, H. Yi, A. Liang, S. He, J. He, Y. Peng, *et al.*, Sci. Rep. **4**, 5385 (2014).
[8] X. Wan, A. M. Turner, A. Vishwanath, and S. Y. Savrasov, Phys. Rev. B **83**, 205101 (2011).
[9] C. Fang, M. J. Gilbert, X. Dai, and B. A. Bernevig, Phys. Rev. Lett. **108**, 266802 (2012).
[10] B. Singh, A. Sharma, H. Lin, M. Z. Hasan, R. Prasad, and A. Bansil, Phys. Rev. B **86**, 115208 (2012).
[11] A. A. Burkov and L. Balents, Phys. Rev. Lett. **107**, 127205 (2011).
[12] M. Ezawa, Phys. Rev. Lett. **116**, 127202 (2016).
[13] Z. Wang, H. Weng, Q. Wu, X. Dai, and Z. Fang, Phys. Rev. B **88**, 125427 (2013).
[14] Y. Du, F. Tang, D. Wang, L. Sheng, E.-j. Kan, C.-G. Duan, S. Y. Savrasov, and X. Wan, arXiv preprint arXiv:1605.07998 (2016).
[15] Q. D. Gibson, L. M. Schoop, L. Muechler, L. S. Xie, M. Hirschberger, N. P. Ong, R. Car, and R. J. Cava, Phys. Rev. B **91**, 205128 (2015).
[16] L. Li, Y. Yu, G. J. Ye, Q. Ge, X. Ou, H. Wu, D. Feng, X. H. Chen, and Y. Zhang, Nat. Nanotech. **9**, 372 (2014).
[17] F. Xia, H. Wang, and Y. Jia, Nat. Commun. **5**, 4458 (2014).
[18] Z. J. Xiang, G. J. Ye, C. Shang, B. Lei, N. Z. Wang, K. S. Yang, D. Y. Liu, F. B. Meng, X. G. Luo, L. J. Zou, Z. Sun, Y. Zhang, and X. H. Chen, Phys. Rev. Lett. **115**, 186403 (2015).
[19] P.-L. Gong, D.-Y. Liu, K.-S. Yang, Z.-J. Xiang, X.-H. Chen, Z. Zeng, S.-Q. Shen, and L.-J. Zou, Phys. Rev. B **93**, 195434 (2016).
[20] A. Morita, Appl. Phys. A **39**, 227 (1986).
[21] Q. Liu, X. Zhang, L. Abdalla, A. Fazzio, and A. Zunger, Nano Lett. **15**, 1222 (2015).
[22] K. Dolui and S. Y. Quek, Sci. Rep **5** (2015).
[23] J. Kim, S. S. Baik, S. H. Ryu, Y. Sohn, S. Park, B.-G. Park, J. Denlinger, Y. Yi, H. J. Choi, and K. S. Kim, Science **349**, 723 (2015).
[24] A. P. Nayak, T. Pandey, D. Voiry, J. Liu, S. T. Moran, A. Sharma, C. Tan, C.-H. Chen, L.-J. Li, M. Chhowalla, J.-F. Lin, A. K. Singh, and D. Akinwande, Nano Lett **15**, 346 (2014).
[25] A. P. Nayak, S. Bhattacharyya, J. Zhu, J. Liu, X. Wu, T. Pandey, C. Jin, A. K. Singh, D. Akinwande, and J.-F. Lin, Nat. Commun. **5**, 3731 (2014).
[26] L. Yang, C.-H. Park, Y.-W. Son, M. L. Cohen, and S. G. Louie, Phys. Rev. Lett. **99**, 186801 (2007).
[27] See Supplemental Material at [URL will be inserted by publisher] for more details about computational details, thermodynamic stability, quantum confinement effect, reduced dimensional effect and symmetry protected Dirac cones, and Dirac cones along different directions.
[28] G. Kresse and J. Furthmüller, Phys. Rev. B **54**, 11169 (1996).
[29] P. E. Blöchl, Phys. Rev. B **50**, 17953 (1994).
[30] J. Klimeš, D. R. Bowler, and A. Michaelides, Phys. Rev. B **83**, 195131 (2011).
[31] X. Fan, C.-H. Chang, W. Zheng, J.-L. Kuo, and D. J. Singh, J. Phys. Chem. C **119**, 10189 (2015).
[32] J. Heyd, G. E. Scuseria, and M. Ernzerhof, J. Chem. Phys. **124**, 219906 (2006).
[33] Y. Akahama, M. Kobayashi, and H. Kawamura, Solid State Commun. **104**, 311 (1997).
[34] S. E. Boulfelfel, G. Seifert, Y. Grin, and S. Leoni, Phys. Rev. B **85**, 014110 (2012).
[35] H. Doh and H. J. Choi, arXiv preprint arXiv:1606.04264 (2016).
[36] J. Zhao, R. Yu, H. Weng, and Z. Fang, Phys. Rev. B **94**, 195104 (2016).

arXiv:1702.06708v1 [cond-mat.mes-hall] 22 Feb 2017

# Supplemental Material for "Layer-Pressure Topological Phase Diagram of Few-Layer Phosphorene"

Peng-Lai Gong,[1,2] Bei Deng,[1] Liang Hu,[1] Wei-Chao Wang,[2] Da-Yong Liu,[3,*] Xing-Qiang Shi,[1,†] Zhi Zeng,[3,4] and Liang-Jian Zou[3,4,‡]

[1] *Department of Physics, Southern University of Science and Technology, Shenzhen 518055, China*
[2] *Department of Electronics and Tianjin Key Laboratory of Photo-Electronic Thin Film Device and Technology, Nankai University, Tianjin 300071, China*
[3] *Key Laboratory of Materials Physics, Institute of Solid State Physics, Chinese Academy of Sciences, P. O. Box 1129, Hefei 230031, China*
[4] *University of Science and Technology of China, Hefei 230026, China*

(Dated: February 23, 2017)

TABLE S1. Structural information and band gap from HSE06 for $n$-layer phosphorene ($n$=2-5) and *bulk* BP under zero pressure. Results in previous theoretical and experimental studies are listed for comparison.

| NL | a (Å) | b (Å) | c (Å) | $d_{int}$ (Å) | $E_g$ (eV) |
|---|---|---|---|---|---|
| 2 | 3.34 (3.33[a]) | 4.47 (4.52[a]) | - | 3.21 (3.20[a]) | 0.95 (1.02[a]) |
| 3 | 3.34 (3.33[a]) | 4.47 (4.51[a]) | - | 3.21 (3.20[a]) | 0.75 (0.79[a]) |
| 4 | 3.34 (3.34[a]) | 4.47 (4.50[a]) | - | 3.21 (3.20[a]) | 0.63 (0.67[a]) |
| 5 | 3.34 (3.34[a]) | 4.47 (4.49[a]) | - | 3.21 (3.20[a]) | 0.58 (0.59[a]) |
| bulk | 3.34 (3.34[a], 3.31[b]) | 4.47 (4.47[a], 4.37[b]) | 10.72 (10.71[a], 10.47[b]) | 3.21 (3.20[a]) | 0.35 (0.36[a], 0.31[b]) |

[a] Ref. [5], theory.
[b] Ref. [6], experiment.

## S1. COMPUTATIONAL DETAILS

First-principles calculations were performed using the projector augmented wave method [1, 2] and a plane-wave basis set as implemented in the Vienna Ab initio Simulation Package (VASP) [2]. In optimizing the geometry of the bulk BP under various pressures, van der Waals interactions were considered by the optB88-vdW functional [3]. The energy cutoff for the plane-wave basis was set to 500 eV for all the calculations. The k-mesh of 13 × 11 × 4 and 13 × 11 in relaxation and electronic structure calculations were adopted to sample the 3D and 2D first Brillouin zone, respectively. The 2D structures under a certain pressure are extracted from the bulk BP under the same pressure. Based on these 2D structures, we carry out the band structures calculations with the hybrid functional of Heyd, Scuseria, and Ernzerhof (HSE06) [4]. The structural information and band-gap values for the 2D structures under zero-pressure are listed in Table S1, as well as one theoretical result with structures by fully-relaxation method [5] and one experimental result [6] for comparison. We find that the band-gap values and structural parameters under zero-pressure are slightly dependent on the obtained structures by the extraction method or the fully-relaxation method. Our results are in agreement with theoretical [5] and experimental [6] results, ensuring that our method is reliable.

## S2. THERMODYNAMIC STABILITY

As the most stable allotrope of phosphorus, bulk black phosphorus exhibits three different phases under moderately high hydrostatic pressures: the orthorhombic phase (A17) with wrinkled hexagons, the graphene-like rhombohedral phase (A7) with hexagonal lattice for the pressure $P > 4.7$ GPa, and the simple cubic phase for $P >$11 GPa [7]. The thermodynamic stability for the bulk BP can be employed to study the structure phase transition, through the enthalpy-pressure relationship for different phases. We calculate the enthalpy-pressure relationship for A17 and A7 phases of the bulk BP in the region of $0 \leq P \leq 5$ GPa in the HSE06 level. As shown in Fig. S1, we find the critical pressure for structure phase transition is 4.6 GPa, in good agreement with the experimental result [7].

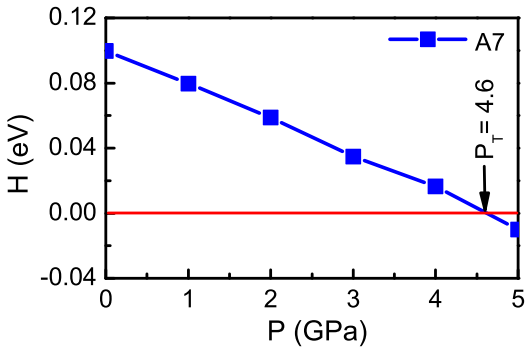


FIG. S1. (Color Online) Relationship of enthalpy and pressure for A17 and A7 phases. A17 and A7 phases are orthorhombic and rhombohedral structures of bulk BP in different regions of pressure. The enthalpy of the A17 phase is set to be zero as a reference to the A7 phase.

## S3. QUANTUM CONFINEMENT EFFECT

For the confinement nanosystems, such as graphene nanoribbons (GNRs), the band-gap values shows clearly size dependence because of the quantum confinement effect (QCE) [8]. Under a hard-wall boundary condition and considering the effective width of GNRs, the formula $E_g$=$a/(w+w_0+\delta_0)$ can well describe the relation of band gap ($E_g$) and the width of 1D GNRs ($w$). As for 2D few-layer phosphorene, the thickness confines the system and influences the band gap. It sholud have a finite band gap when the thickness is approaching the bulk below the critical pressure of 1.2 GPa. Therefore, we use a modified formula

$$E_g = \frac{a}{w+b} + c \tag{1}$$

to fit the band gap values in Fig. S2 (a), and then get the fitted results

$$\begin{aligned} E_g^{P=0.0} &= \frac{8.37}{w^{P=0.0}+4.91} + 0.28 \\ E_g^{P=1.0} &= \frac{8.90}{w^{P=1.0}+4.66} + 0.07 \end{aligned} \tag{2}$$

Our results show that the size dependence of band gaps for the pressured few-layer phosphorene (in case of $P$=0.0 and 1.0 GPa) can be well expressed by an inverse relation (1). Based on the structural information under $P$ = 0.0 and 1.0 GPa, we obtain the relationships between $w$ and $n$:

$$\begin{aligned} w^{P=0.0} &= 5.37 \cdot n - 3.21 \\ w^{P=1.0} &= 5.26 \cdot n - 3.10 \end{aligned} \tag{3}$$

where $n$ is the number of layers ($n \geq 2$). The slope $k$=$dE_g/dP$ (the absolute value) can be expressed by

$$\begin{aligned} k &= \left| \frac{E_g^{P=0.0} - E_g^{P=1.0}}{\triangle P} \right| \\ &= \frac{8.37}{w^{P=0.0}+4.91} - \frac{8.90}{w^{P=1.0}+4.66} + 0.21 \end{aligned} \tag{4}$$

According to (3) and (4), $k$ can be directly relative to $n$:

$$k = \frac{8.37}{5.37 \cdot n + 1.70} - \frac{8.90}{5.26 \cdot n + 1.56} + 0.21 \tag{5}$$

As shown in Fig. S2 (b), the band gap change rate $dE_g/dP$ increases with increasing layers, owing to the decreased QCE in thicker layers. The decreased slope $k = dE_g/dP$ in few-layer phosphorene resists the band-gap reduction, which, together with the QCE-induced larger gap, leads to the band-gap closing at a higher $P_C$ than expected. Here, we define the difference between the critical pressures with the inclusion and exclusion of QCE as $\triangle P = P_C$-$P'_C$, which can reflect the QCE on the ideal critical pressure $P'_C$ for TPTs. From Fig. S2 (c), we find that $\triangle P$ decreases with the increasing of layers, indicating the QCE can be significantly reduced in thicker layers. For example, the contributions of $\triangle P$ to $P'_C$ are 50% for 4 layers and 33% for 6 layers, respectively.

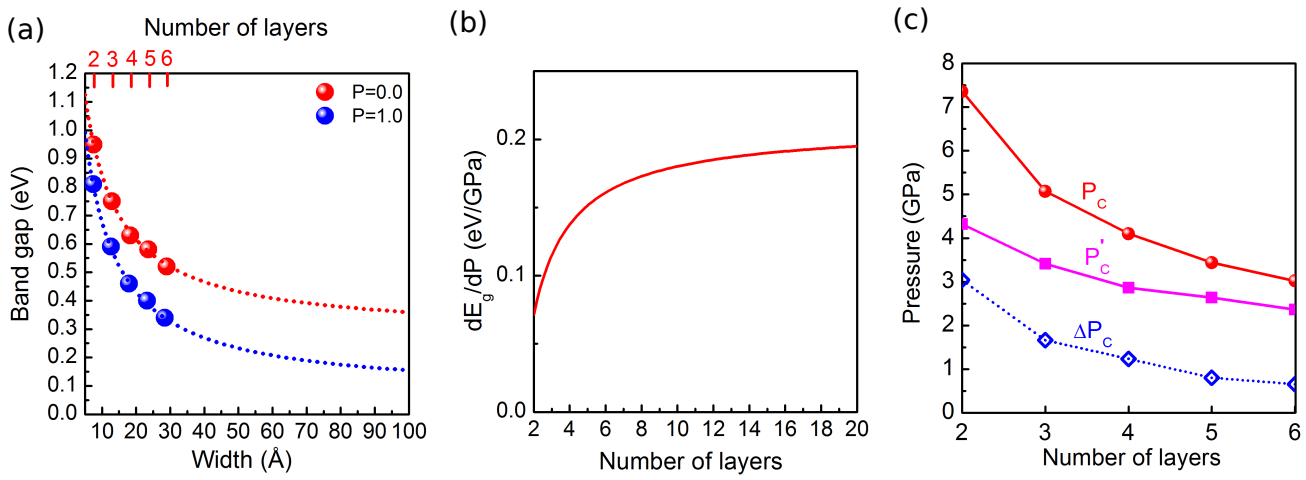


FIG. S2. (Color Online) (a) Band-gap values at $P$=0.0 (red) and $P$=1.0 GPa (blue) as a function of the confinement size. The widths and its corresponding layers for $P$=0.0 GPa are illustrated. The fitted curves (red and blue dashed lines) are obtained according to the formula $E_g$=a/(w+b)+c, where a, b and c are fitted parameters. (b) The slope $k$ as a function of the number of layers. (c) $P_C$, $P'_C$ and $\triangle P$ as a function of the number of layers. $P_C$ and $P'_C$ denotes the critical pressures with the inclusion and exclusion of QCE (see Fig. 4 (b) in main text), here we define $\triangle P$ =$P_C$-$P'_C$.

## S4. REDUCED DIMENSIONAL EFFECT AND SYMMETRY PROTECTED DIRAC CONES

Some symmetry elements for few-layer phosphorene and *bulk* BP are listed in Table S2. Odd-layer, even-layer phosphorene and bulk BP preserve glide planes and screw axis, and their space groups do not change under pressures. Some symmetry elements for 4-layer phosphorene, with particular deformations under 4.4 GPa, are listed in Table S3. Dirac cones are protected by the nonsymmorphic space symmetry (YZ glide plane at the middle of the zigzag chain) of quasi-two-dimensional phosphorene.

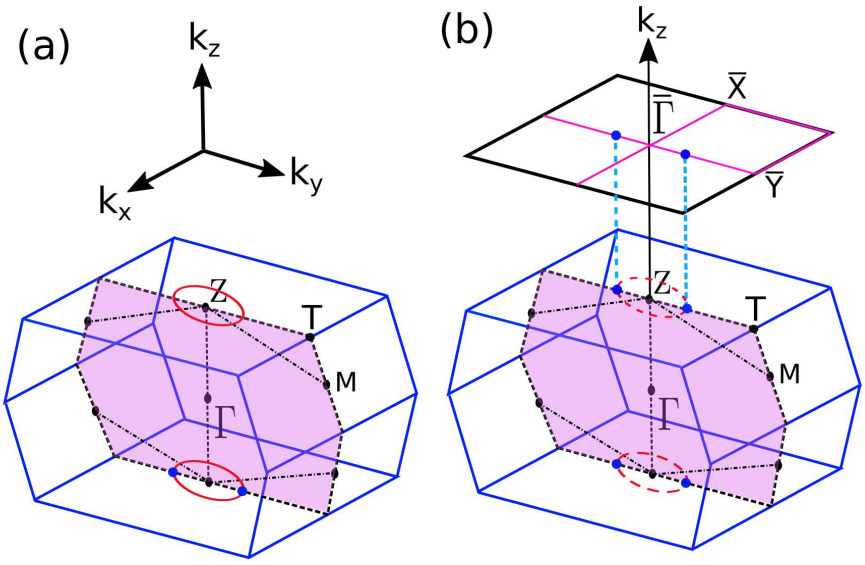


FIG. S3. (Color Online) Sketched distribution of Dirac cones in the first Brillouin zone of *bulk* black phosphorus (bottom) and few-layer phosphorene (top) in semimetal state without SOC (a) and with SOC (b). The projected surface BZ is shown (top in (b)).

TABLE S2. Some symmetry elements for few-layer phosphorene and *bulk* BP.

| | glide | screw axis | inversion | point group | space group |
|---|---|---|---|---|---|
| bulk | YZ, XY, XZ | X,Y,Z | YES | D2H-18 | CMCA |
| odd layer | YZ, XY | X | YES | D2H-7 | PMNA |
| even layer | YZ, XY | X | YES | D2H-11 | PMCA |

TABLE S3. Some symmetry elements for 4-layer phosphorene after particular deformations.

| | glide | screw axis | inversion | point group | space group | dirac |
|---|---|---|---|---|---|---|
| no translation | YZ, XY | X | YES | D2H-11 | PMCA | YES |
| t(x) | NO | NO | NO | CS-1 | PM | NO |
| t(y) | YZ | Z | YES | C2H-5 | $P2_1/A$ | YES |
| t(z) | YZ | Y | NO | C2V-4 | PMA2 | YES |

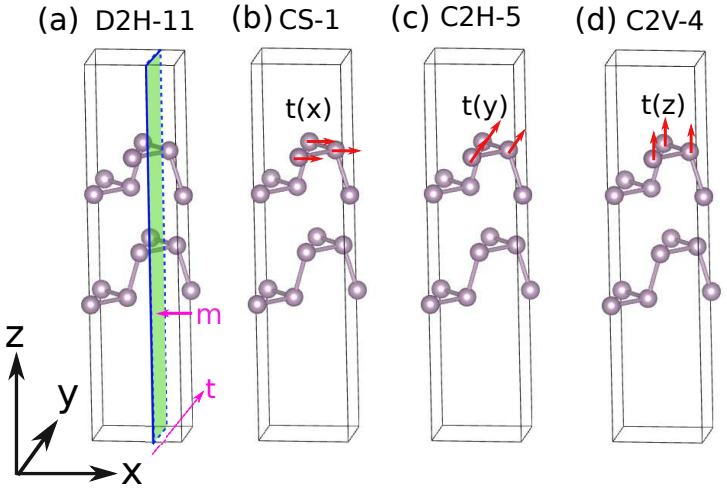


FIG. S4. (Color Online) Illustration of few-layer phosphorene (a) without deformations and (b-d) with particular deformations. Move the outmost P atoms by 0.1 Å along (b) x, (c) y and (d) z directions, respectively. $t(x)$, $t(y)$ and $t(z)$ are translation vectors, and point group for the structures are shown. The glide plane (green) in (a) is displayed, where operate $m$ and $t$ denote the mirror and translation vector.

## S5. DIRAC CONES ALONG DIFFERENT DIRECTIONS

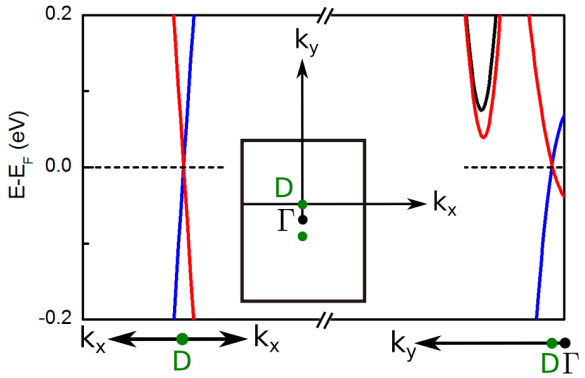


FIG. S5. (Color Online) Band structures (with SOC) of 4-layer phosphoren at 4.4 GPa along the $k_x$ and $k_y$ directions around the Dirac point. Dirac point (denoted by green point, labeled with "D") was set to be the origin in the band structure plot.

* dyliu@theory.issp.ac.cn
† shixq@sustc.edu.cn
‡ zou@theory.issp.ac.cn

[1] P. E. Blöchl, Phys. Rev. B **50**, 17953 (1994).
[2] G. Kresse and J. Furthmüller, Phys. Rev. B **54**, 11169 (1996).
[3] J. Klimeš, D. R. Bowler, and A. Michaelides, Phys. Rev. B **83**, 195131 (2011).
[4] J. Heyd, G. E. Scuseria, and M. Ernzerhof, J. Chem. Phys. **124**, 219906 (2006).
[5] J. Qiao, X. Kong, Z.-X. Hu, F. Yang, and W. Ji, Nat. Commun. **5**, 4475 (2014).
[6] L. Cartz, S. Srinivasa, R. Riedner, J. Jorgensen, and T. Worlton, J. Chem. Phys. **71**, 1718 (1979).
[7] Y. Akahama, M. Kobayashi, and H. Kawamura, Solid State Commun. **104**, 311 (1997).
[8] L. Yang, C.-H. Park, Y.-W. Son, M. L. Cohen, and S. G. Louie, Phys. Rev. Lett. **99**, 186801 (2007).